**Proceedings of IMECE2007**
**2007 ASME International Mechanical Engineering Congress and Exposition**
**November 11-15, 2007, Seattle, Washington, USA**

# IMECE2007-43878

# MICRO/NANOSCALE STRUCTURE FABRICATION BY DIRECT NANOIMPRINTING OF METALLIC AND SEMICONDUCTING NANOPARTICLES

**Inkyu Park**
Berkeley Sensor and Actuator Center (BSAC)
Mechanical Engineering Department
UC Berkeley, Berkeley, CA 94720

**Seung H. Ko**
Mechanical Engineering Department
UC Berkeley, Berkeley, CA 94720

**Heng Pan**
Mechanical Engineering Department
UC Berkeley, Berkeley, CA 94720

**Albert P. Pisano**
Berkeley Sensor and Actuator Center (BSAC)
Mechanical Engineering Department
UC Berkeley, Berkeley, CA 94720

**Costas P. Grigoropoulos**
Mechanical Engineering Department
UC Berkeley, Berkeley, CA 94720

## ABSTRACT

In this paper, we present our recent development of direct nanoimprinting of metal and semiconductor nanoparticles for a simple but high-throughput fabrication of micro/nanoscale structures. Nanoparticle suspension with self-assembled-monolayer (SAM) protected-nanoparticles (Au, Ag, and CdSe-ZnS core-shell quantum dots) suspended in alpha-terpineol carrier solvent are used as solutions for direct nanoimprinting. Polydimethylsiloxane (PDMS)-based soft imprinting molds with micro/nanoscale features are used. Process and material flexibility enable a very low temperature (80 ºC) and low pressure (5psi) nanoimprinting process and results in superfine features from micrometers down to ~100nm resolutions. We will show the geometrical and electrical characterization of nanoimprinted structures and demonstrate working electronic components such as resistors or organic field effect transistors (OFET).

## INTRODUCTION

Recently, nanoimprinting has been introduced as an inexpensive and high-throughput nanopatterning method [1-6]. This is becoming an alternative method to other approaches (eg. electron-beam lithography, extreme-UV lithography, etc) that require expensive and complicated setups. The basic principle of nanoimprinting is very simple: First, nanoimprinting mold is machined by other nanolithography method (eg. electron-beam lithography). Second, imprinting resist is deposited on the substrate and mold is placed upon the imprinting resist. Third, pressure and temperature (thermal embossing type) or additional optical energy (UV imprinting type) is applied. Last, after removing the imprinting mold, the imprinted patterns are used as either as active structures or mask layers for further processing (eg. etching, metal lift-off, etc.) Although an initial cost is required for mold fabrication, the imprinting process itself is very economical and simple compared to other methods. Due to these advantages, their applications are expanding from nanoscale electronics [4-6] to optical components [2,3] and to biofunctional nanostructures [7].

One of the most important nanopatterning is that of metallic layers. Metal patterns are used as electrical interconnection elements or electrodes in the electrical applications. Also, nanoscale metal islands are used as sensor platforms for the optical biosensing such as surface enhanced Raman spectroscopy (SERS) [8]. Usually the nanoscale metal patterns have been made by indirect method [9]: Polymer (e.g. PMMA) pattern is first created by nanoimprinting, which is then used as mask for dry etching of a predeposited metal film or as part of the metal lift-off process. As one can see, conventional metal nanoimprinting involves multiple steps and

expensive processes, thereby increasing the cost of manufacturing and offsetting the advantages of the nanoimprinting process. Very few direct metal nanoimprinting processes have been demonstrated so far due to the high melting temperature of metals. As alternatives to metal direct nanoimprinting, a few solid state embossing methods based on plastic deformation of metal thin films have been introduced. These approaches involved either deformation of metal film under very high pressure [10] or deformation of a metal thin film/polymer multilayer under lower pressure [11]. Evidently, these processes are limited by the fact that the metal is still in the solid state. Either ultra-high pressures, or metal/polymer multilayers, and sharp mold geometries are required to deform the metallic layer. The high pressures damage the substrate, and the sharp mold geometries are difficult to fabricate. Additionally, these methods do not allow the fabrication of isolated, arbitrary features, and always leave unwanted residual polymer layers.

We have developed a novel method of direct nanoscale metal patterning by nanoimprinting of imprinting solutions of metal nanoparticle suspended in organic solvents [12]. The metal nanoparticles whose diameter spans from 2 to 5 nm are chemically synthesized by two-phase reduction method and encapsulated with a self-assembled monolayer of organic surfactant. By suspending these particles in organic solvents (eg. α-terpineol) in an appropriate concentration, one can adjust the fluidic viscosity of the imprinting solution. Due to great temperature sensitivity of fluidic viscosity, this metal nanoparticle solutions can be easily imprinted at low temperature (eg. 80ºC), low pressure (5psi) conditions – which are lower than conventional thermal embossing process by several factors. Therefore, the requirement of process equipment and manufacturing cost are dramatically lessened accordingly. Another advantage of this low temperature / pressure conditions is that one can use flexible imprinting mold such as poly(dimethylsiloxane) (PDMS) that is much easier to replicate than rigid molds such as silicon or quartz. Another advantages of PDMS mold are that it allows the evaporation of organic solvents and that it greatly contributes to the residual layer minimization due to the great conformal contact between the PDMS mold and the substrate [13] during the nanoimprinting process. After the imprinting process, the imprinted micro / nanostructures of metallic nanoparticle clusters are melted by heating at moderate temperatures (eg. 140ºC). During this thermal treatment process, a collection of individual metal nanoparticles are gathered and transformed into a continous metallic film. Procedures of direct nanoimprinting process of metallic nanoparticles are depicted in Figure 1. Since the specific nanoparticle material does not significantly change the fluidic properties of the nanoparticle solution, the nanoimprinting process developed in this work is quite versatile and hence can be used for a variety of metallic or semiconducting nanoparticles with little process modification. Herein we have applied this method to gold (Au) and silver (Ag) nanoparticles, and cadmium selenide-zinc sulfide (CdSe-ZnS core-shell) nanocrystals. Micro/nanoscale patterning of semiconducting nanocrystals (i.e. quantum dots) such as CdSe-ZnS core-shell nanocrystals is expected to provide oppotunities in a number of biosensing applications such as fluorescence resonance energy transfer (FRET)-based optical biomolecule sensing [14].

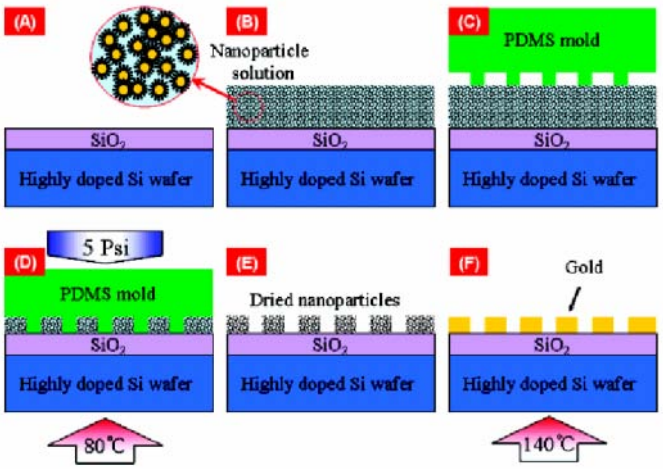


Figure 1. Direct nanoimprinting process of metal nanoparticles. (A,B) Dispensing nanoparticle solution on substrate (C,D) Pressing mold and applying heat & pressure (E,F) Removal of mold and melting of nanoparticles into continuous, conductive pattern. Nanoimprinting of semiconducting nanocrystals does not have step (F).

## EXPERIMENTAL

*Nanoparticle solution preparation*

The gold nanoparticles were prepared by a two-phase reduction method reported by Hostetler *et al.* [15]. Aqueous metal salts ($HAuCl_4$) were mixed in a toluene solution containing long-chain alkylammonium surfactants to form a two-phase system. 1.5g of tetroactylammonium bromide ($C_{32}H_{68}BrN$) was mixed with 80 mL of toluene and added to 0.31 g of Hydrogen tetrachloroaurate (III) hydrate ($HAuCl_4 :xH_2O$) in 25 mL of deionized (DI) water. Vigorous stirring transfered the metal salt ($AuCl_4^-$) into the organic phase (toluene) and the aqueous phase was removed. A measured quantity of capping agent, a long-chain thiol (Hexanethiol), was added to the gold solution while stirring. Then, a reducing agent, sodium borohydride ($NaBH_4$), mixed in 25 mL of water was added into the organic phase with a fast addition over approximately 10 s to nucleate nano-crystals. The mixture reacted at room temperature for 3.5 hours. The toluene was removed with a rotary evaporator and the leftover black particles suspended in ethanol and sonicated briefly. The particles were washed with ethanol and acetone and air dried. The average size of synthesized gold nanoparticles was measured to be 1~3nm from the TEM observation. The synthesized gold nanoparticles were mixed well with α-

terpineol solvent (10 wt. %) by ultrasonication for the usage as nanoimprinitng solution. Monodisperse silver nanoparticles (3-7nm diameter in average) were purchased from ULVAC, Inc (Japan). The composition of silver nanoparticle dispersion was 35 parts (by weight) silver nanoparticles, 7 parts dodecylamine as alkylamine, and 58 parts of toluene as an organic solvent. This nanoparticle dispersion was further mixed with α-terpineol solvent so that silver concentration is decreased to 10 wt. %. For uniform mixture of the solution, microvortexer and ultrasonication were employed. Cadmium selenide-zinc sulfide (CdSe-ZnS; core-shell) nanocrystals were obtained from Evident Technologies, Inc. (Troy, NY). The nanocrystals were dispersed in hexane solvent and had emission peak at 620nm (maple red-orange color emission). This solution was mixed with α-terpineol solvent by 1:1 composition for the usage as a nanoimprinting fluid.

*Nanoimprinting Mold Fabrication*

The fabrication of PDMS mold with microscale patterns was performed by the following procedure: (1) The silicon wafer was cleaned with piranha solution and with an $O_2$ plasma, and treated with SAM hexamethyldisilazane (HMDS) to enhance the adhesion of photoresist on the substrate. (2) 1.3 μm thick G-line positive photoresist (OCG825, Arch Chemicals, Inc., Columbus, OH) was spin coated onto the silicon wafer. (3) 4x reduction lithography (FPA-141F, Canon Inc., Japan) was used for the patterning of microscale features followed by developing with G-line developer (OCG 934, Arch Chemicals, Inc.). (4) After hardbaking at 120 °C, the silicon master was coated with 10 nm thick polytetrafluoroethylene (PTFE) using a vapor phase deposition system (Advanced Silicon Etch System, Surface Technology Systems, UK) to prevent the stiction of PDMS to the silicon master. (5) 10:1 (PDMS : curing agent) mixture of Sylgard 184 silicone elastomer kit (Dow Corning, Midland, MI) was poured on the silicon master. (6) It was degassed at room temperature and atmospheric pressure for 1 h and cured at 70 °C for 2 h. (7) After curing, the PDMS mold was carefully released from silicon master. For the fabrication of mold with nanoscale features, steps (1)-(3) were replaced with electron-beam lithography on 200nm thick Poly(methyl methacrylate) (PMMA) followed by electron beam deposition and lift-off of 50nm thick Cr/Pt/Ti layers.

*Nanoimprinting Process*

The nanoimprinting process was carried out in the following procedures: First, silicon-based substrates were prepared. Moderately doped bare silicon wafers were used for simple nanoimprinting tests, while highly-doped p-type silicon wafer (< 0.005Ω/cm) with 100nm thick thermal $SiO_2$ was used for electrical device fabrication and tests such as OFET (organic field effect transistor) device. The substrates were cleaned in piranha solution and dehydrated at 120℃ for 10 minutes. The gold nanoparticles (1~3 nm diameter) and silver nanoparticles (3-7nm diameter) encapsulated by hexanethiol SAM (self assembled monolayer) in an α-terpineol solvent (10 wt. %) were dispensed on the substrate heated at 80℃ to optimize nanoparticle ink viscosity and surface tension for faithful nanoimprinting patterning and minimum residual layer. PDMS mold was placed on top of nanoparticle solution with and small pressure (5 psi) and moderate heat (80℃) was applied for 20mins to let the nanoimprinting solution flow and fill the features and evaporate organic carrier solvent. The substrate was cooled down to room temperature for 1 hour to assure complete cooling and PDMS mold was removed to get patterned nanoparticle. Finally, sample with nanoparticle pattern was heated at 140℃ (for gold nanoparticles) and 180℃ (for silver nanoparticles) for 2 hours to induce nanoparticle melting to transform the nanoparticle clusters to continuous conductor pattern. For the fabrication of organic field effect transistor (OFET), a spin coating process of semiconducting polymer was added as the last step. The nanoimprinting of CdSe-ZnS nanocrystals was done in similar process except that the curing process at 140-180℃ are not required. Only moderate heating (80℃) during the nanoimprinting process allowed the complete evaporation of toluene solvent and formation of dry patterns of CdSe-ZnS nanocrystal clusters.

*Preparation of Air-stable Semiconducting Polymer*

The air-stable semiconducting polymer used in this research is a novel material of a modified polythiophene containing electron withdrawing alkyl carboxylate substituents, exhibiting high charge mobility. All chemicals were purchased from Aldrich and used without further purification unless otherwise noted. All solvents were purified on a solvent purification system. All reactions were performed under $N_2$ unless otherwise noted. All extracts were dried over anhydrous $MgSO_4$ and solvents were removed by rotary evaporation with vacuum assist. Flash chromatography was performed using Merck Kieselge l60 (230 - 400 mesh) silica. The detailed semiconducting polymer synthesis and characterization can be found in the reference [16].

*Sample Characterization*

Sample characterization mainly comprises two parts: surface & topological characterization and electrical characterization. Surface characterization of the fabricated samples was done by optical microscopy (BX-60, Olympus Inc.), scanning electron microscopy (SEM, LEO 1550, Carl Zeiss, Inc.), atomic force microscopy (AFM, Dimension 3100, Veeco Instruments), Energy Dispersive X-ray analysis (SEM-EDX, Gemini Ultra-55, Carl Zeiss, Inc.), and X-ray Photoelectron Spectroscopy (XPS, PHI 5400, Physical Electronics, Inc.). Electrical characterization such as electrical resistivity of conductive structures and standard transistor testing were done by semiconductor analyzer (HP 4155, Hewlett-Packard Co.).

## RESULTS & DISCUSSION

*Thin Films derived from Nanoparticle Solution (Gold NP)*

The surface characteristics of thin films derived from nanoparticle solution is critical for properties of imprinted structures in terms of surface topology, electrical conductivity, etc. The film characteristics change dramatically by heating temperatures and periods. We have investigated the characteristics of the gold thin film derived from gold nanoparticles in the aspects of chemical composition, surface morphology, and electrical conductivity. In particular, samples heated at 140 ºC for different periods were characterized. This temperature was chosen from a series of thermal treatment testing at different temperatures: 30 ºC, 50 ºC, 120 ºC, 140 ºC, and 180 ºC. Dependence of electrical resistivity of the gold nanoparticle-based film on the heating temperature is shown in Figure 2. Low temperatures such as 30-50 ºC did not allow the evaporation of α-terpineol solution even after 2 days of heating. Sample heated at 120 ºC also exhibited a very high electrical resistivity, representing an incomplete melting. As the film is heated above 150 ºC, the resistivity approaches to the bulk values. However, heating at high temperature (eg. 180 ºC) caused a severe cracking of gold thin films, which is undesirable. A clean, highly reflective, and smooth gold thin film with no crack was obtained by heating at 140 ºC for an extended period of time (2 hours).

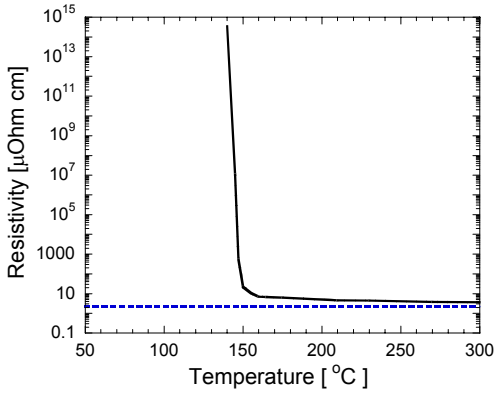


Figure 2. Resistivity of gold nanoparticle-based thin films. Blue dotted line represents bulk gold resistivity (2.65μΩ·cm)

The change of chemical composition and surface morphology in gold nanoparticle film by the heating at 140 ºC for different time periods was investigated. As seen in Figure 3(A), gold (Au), carbon (C), and sulfur (S) are three main components of the gold nanoparticle film. Gold (Au) is the core element for gold nanoparticles while carbon (C) and sulfur (S) exist in the hexanethiol SAM layer and α-terpineol solution. By heat treatment for longer periods, the composition of gold (Au) and carbon (C) does not change significantly. However, sulfur (S) from thiol group is eliminated from the surface after 7 hours of heating. Figure 3(B) exhibits the change of surface morphology of gold nanoparticle film. After 30 minutes of heating, the surface is quite rough ($R_{ms}$=0.89nm, $R_{max}$=7.493nm). After 2 hours of heating, the film turns out very smooth ($R_{ms}$=0.16nm, $R_{max}$=1.29nm). After 7 hours of heating, the surface becomes very rough again ($R_{ms}$=2.26nm and $R_{max}$=18.639nm) with some visible nano-sized grooves (width=150nm, depth=8.71nm). It is believed that this surface roughening originates from the surface stress by agglomeration of gold nanoparticles. From this observation, 2 hours is found to be an optimal heat treatment period in terms of surface morphology. Also, the electrical resistivity of gold nanoparticle film does not decrease any further after 2 hours of heating. Therefore, we have chosen 2 hours and 140 ºC as the heating time and temperature in the melting process after nanoimprinting of gold nanoparticles. This surface characterization was done only for the gold nanoparticle thin film in this paper, but can be extended to silver nanoparticle and semiconductor nanocrystal thin film samples as potential future works.

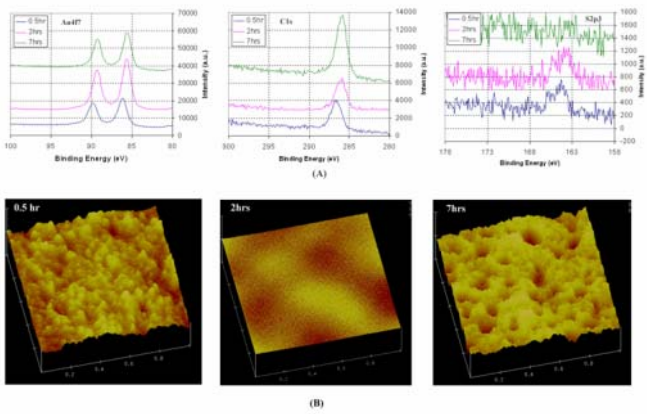


Figure 3. Change of surface chemistry and morphology by heat treatment of gold nanoparticle-based thin film at 140 ºC for different periods (30(A) XPS analysis of Au4f7, C1s, s2p3 peaks (B) AFM scanning image of gold nanoparticle-based thin film after heating process.

*Micro & Nanostructures of Nanoparticles by Nanoimprinting*

Various micro/nanoscale features have been fabricated by the direct nanoimprinting process. AFM images and cross sections of gold nanowires with 450 nm width (FWHM, 4 μm pitch) and 280 nm height are shown in Figure 4(A). Optical dark field / bright field microscope images of microwires of various widths and pitch are presented in Figure 4(B) (1/2/4/6/12/14/30 μm line with and 4/8/8/16/16/16/32 μm pitch from (i) to (vii), darkfield: top row, bright field: bottom row). The AFM topography images (Figure 4(C)) and optical darkfield (left half) and bright field (right half) microscope images (Figure 4(D)) of imprinted positive and negative micron sized features are shown. Square positive features (from negative mold) are shown in diverse size and density (Figure 4(C)-i: 2.7 μm width and 8 μm pitch, Figure 4(D)-i, ii: 3/6 μm width and 16 μm pitch, 200 nm high) while square and circular negative features (from positive mold) are shown in diverse

size and density (Figure 4(C)-ii, iii: 2.4/4.6 μm width and 8/16 μm pitch, Figure 4(D)-iii, iv: 3/6 μm width and 16 μm pitch, 200 nm high). Similar results can be obtained by direct nanoimprinting of silver nanoparticles as shown in Figure 5.

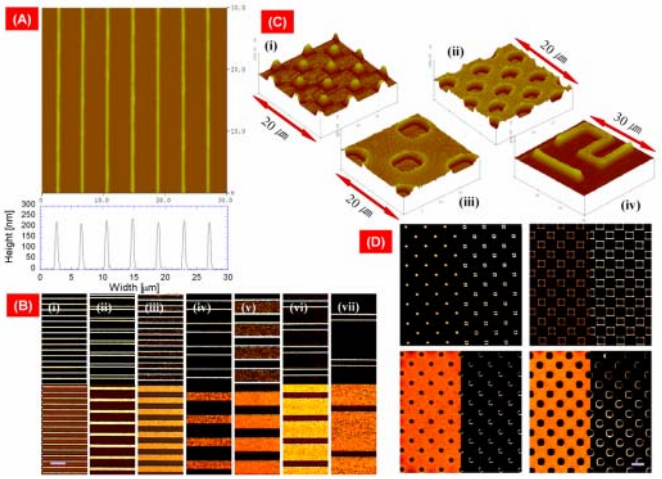


Figure 4. Nanoimprinted gold nano/micro features. AFM topography images of (A) nanowire arrays, (C-i) positive micro dot arrays, (C-ii,iii) negative micro dot arrays and (C-iv) letters. Optical images of (B) microwire arrays (top row: dark field, bottom row: bright field), (D-i,ii) positive micro dots and (D-iii,iv) negative micro dots (left column: dark field, right row: bright field). Inset scale bars correspond to 10μm.

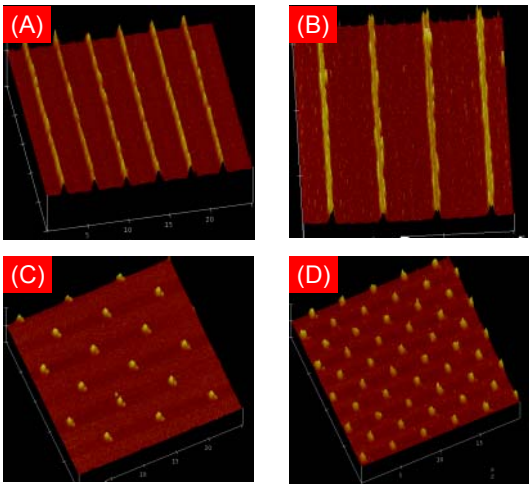


Figure 5. Nanoimprinted silver (Ag) micro features. AFM topography images of (A),(B) microwire arrays (1μm line width / 4μm pitch ; 2μm line width / 8μm pitch), (C,D) microdot arrays (1μm width, 8μm pitch ; 1μm width, 4 μm pitch)

Nanoscale structures have also been fabricated by direct nanoimprinting process. Diverse gold structure (nanodots, nanowires and nanomeanders) arrays with varying sizes (down to 100 nm), densities, and aspect ratios was demonstrated as shown in Figure 6. Figure 6(A) shows optical darkfield microscope images of arrays of 200 nm (6(A)-ii,iv,v, 400 nm

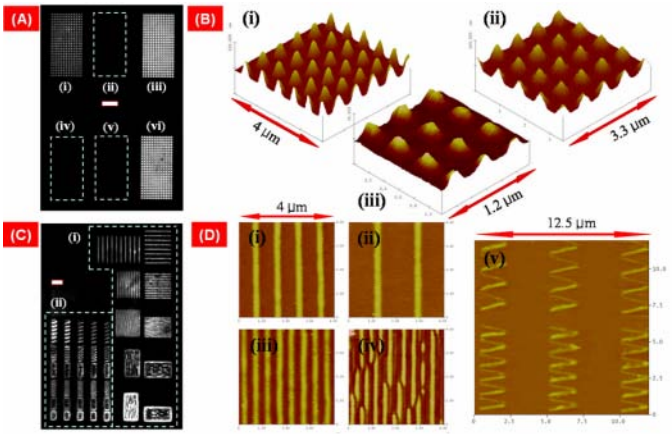


Figure 6. Nanoimprinted gold nanofeatures. Optical dark field images of (A) nanodots and (C) nanowires (inset scale bar corresponds to 5μm). AFM topography images of (B) nanodots, (D(i~iv)) straight nanowires and (D(v)) serpentine nanowires.

pitch) and 400 nm (6(A)-i,iii,vi, 800 nm pitch) sized nanodots with 3 different shapes (6(A)-i,iv: circular, 5(A)-ii,iii: diamond, 6(A)-v,vi: square). While 400 nm dot arrays are clearly visible, 200 nm dots could not be easily observed at the same illumination light intensity because smaller dots scatter less light. The atomic force microscopy (AFM) topography images of the nanodot arrays are shown in Figure 6(B). Arrays of square shaped (Figure 6(B)-i, iii) and circular shaped (Figure 6(B)-ii) nanodots of width in the range of 130-250 nm (FWHM) with heights of 8-50 nm depending upon the width were successfully fabricated by nanoimprinting process. Precise control of localization and pattern replication were achieved with high fidelity and negligible or no residual layer. In Figure 6(C) and (D) are shown one-dimensional nanowires made by nanoimprinting. Figure 6(C) shows optical darkfield microscope images of 100 nm wide (nominal) nanowire arrays with different pitch (6(C)-i, 200/300/500/900/1700 nm pitch from the bottom) and meandering nanowires (6(A)-ii, 24 μm total length). The AFM topography images of the nanowire arrays are shown in Figure 6(D). Nanowire arrays with relatively larger pitch (down to 300 nm pitch) can imprint 200 nm (FWHM) clean nanowires without discontinuity (Figure 6(D)-i~iii). However, 200 nm pitch nanowire imprinting (Figure 6(D)-iv) shows local line discontinuities that may be a result of incomplete filling at the nanoscale, the line width broadening by possibly material diffusive spreading and expansion of trapped air or moisture.[12] This is more serious when the line width becomes comparable with the pitch. This pattern expansion limits the pattern density and reduces resolution. Besides straight nanowires, meandering nanowires (Figure 6(D)-v) were printed successfully without discontinuity.

After the nanoimprinted metal nanoparticles are melted and sintered on a hot plate, the nanofeatures show tapered sidewalls and vertical shrinkage compared to feature depths of PDMS mold. These may be due to either reflow of the

nanoparticle solution and densification during the melting process, incomplete filling of metal nanoparticle solution into the PDMS mold, or deformation of PDMS mold by the applied pressure. Similar influence of densification and Poisson's ratio of nanoimprinted polymers on the cross section of the fabricated features has been reported [9]. Significant deviation in the sidewall angle from vertical can change the line width during the nanoparticle melting. As the aspect ratio becomes small, the sidewall angle degradation becomes more severe for the isolated dots than for the nanowire features. The maximum aspect ratio that can be obtained is highly dependent on the size and shape of the features. In this work, we could obtain aspect ratios as large as 1/3. Because of the elastomeric behavior of the material, the aspect ratio decreased in the case of small or isolated structures.

The imprinting of large and isolated array features surrounded by large unstructured areas is challenging in terms of complete filling of the fluid in the PDMS mold and minimizing the residual layer [9]. This is true for either elevated features or cavities and becomes more critical as the size becomes smaller. We strived to solve this problem by designing microscale dummy features near the active nanoscale structures and by dispensing precise quantities of the nanoparticle solution. This could help both minimize residual layers and achieve uniform filling of nanoparticle solutions in the nanoscale features across the entire imprinting mold area. The residual layers were analyzed by energy dispersive X-ray analysis (EDX), electrical measurement, optical image, and AFM scanning. These diagnostics showed absence or insignificant amount of residual layer in the imprinted area. In particular, electrical measurements assured that neighboring nanowires are electrically isolated, thereby proving that there are no continuous and conductive left-over residual layers that may cause leakage current. SEM-EDX analysis shown in Figure 7 also verified that the quantity of residual layer between desired imprinting features are negligible. SEM-EDX images were taken for nanoimprinted gold nanoparticle structures – line arrays and hole arrays. Comparison of SEM image (Figure 7(A)) and EDX mapping image of gold (Au) element (Figure 7(B)) shows that the amount of residual layer is negligible. Moderate heating during the nanoimprinting process allows the nanoparticle solution to have a low viscosity. This, along with conformal PDMS mold – substrate surface contact, facilitates the complete pattern replication with minimum residual layer.

The CdSe-ZnS core-shell nanocrystals (quantum dots) have also been patterned by using direct nanoimprinting process. In order to verify that the fluorescent behaviors of original quantum dots are maintained after the nanoimprinting process, we have excited the sample with Ar ion laser (principal emissions at 488 and 514nm wavelength) and took the pattern image emitted from the sample and filtered through 620nm emission filter. As shown in Figure 8, maple red-orange fluorescence is emitted from nanoimprinted patterns of quantum dots without any noticeable light intensity decrease (photobleaching). As we changed the emission filter to other wavelengths (eg. blue or green), no fluorescence image could be observed. Therefore, it can be concluded that the fluorescence properties of quantum dots with sharp fluorescence spectra with no photobleaching is maintained after the nanoimprinting process.

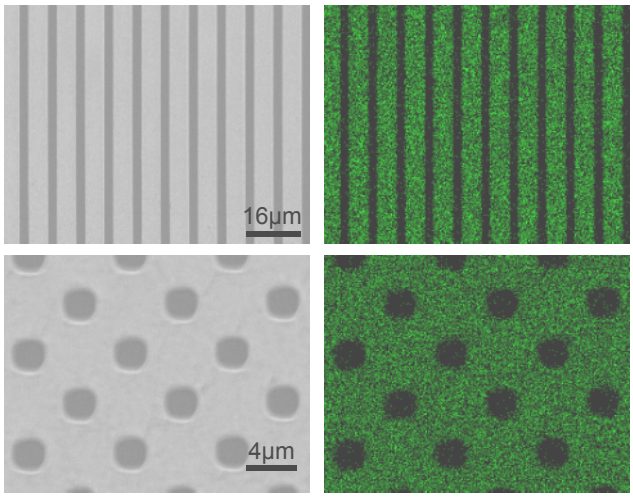


Figure 7. Energy dispersive X-ray (EDX) analysis of nanoimprinted gold (Au) nanoparticle structures. (A) SEM images and (B) EDX mapping images of line and hole arrays show that the amount of residual layer is negligible.

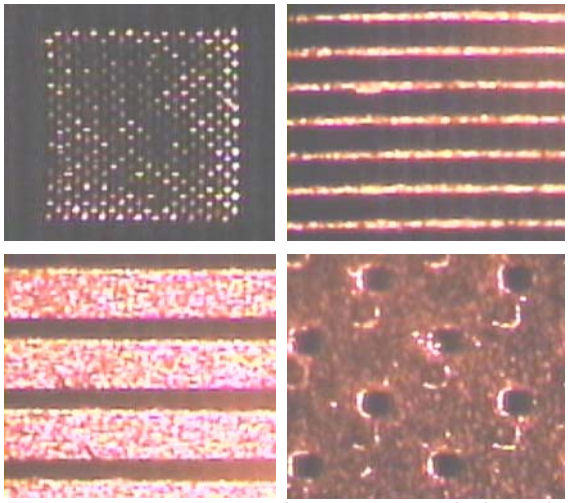

Figure 8. Fluorescence image of nanoimprinted CdSe-ZnS core-shell nanocrystals (quantum dots). Excitation at 488-514nm wavelength with Ar ion laser and emission at 620nm wavelength. Unique fluorescent characteristics of quantum dots (sharp fluorescence spectra with negligible photobleaching) are maintained in the nanoimprinted structures of quantum dots.

*Electronic Device Fabrication & Its Characterization*

The electrical properties of the nanoimprinted features are crucial for their actual use in the micro/nano-electronics applications. Two types of resistivity test configurations –

single line resistors as shown in Figure 9 (A)-i (optical dark field image) and Figure 9(C) (AFM image) and multiple line resistors as shown in Figure 9(A)-ii (optical dark field image) and Figure 9(D) (AFM image) – were fabricated by direct nanoimprinting process. The resistivity ($\rho$) is calculated from $\rho = R \cdot A/L$. The resistance $R$ was measured with a micro needle probe station. $A$ is the cross sectional area of the gold line measured from AFM scanning data and $L$ is the length of the test sample (200 μm). The measured resistivity (30 μΩ.cm) obtained from nanoimprinting was almost one order higher than the bulk value (2.65 μΩ.cm, solid line in Figure 2) but it was still sufficiently conductive for high performance electronics. This resistivity value difference could be explained by enhanced carrier scattering in the presence of a polycrystalline structure, rough surface ($R_{rms}$ ~ 5 nm), and incomplete desorption of hexanethiol layer between gold nanoparticles that would then act as a dielectric layer.

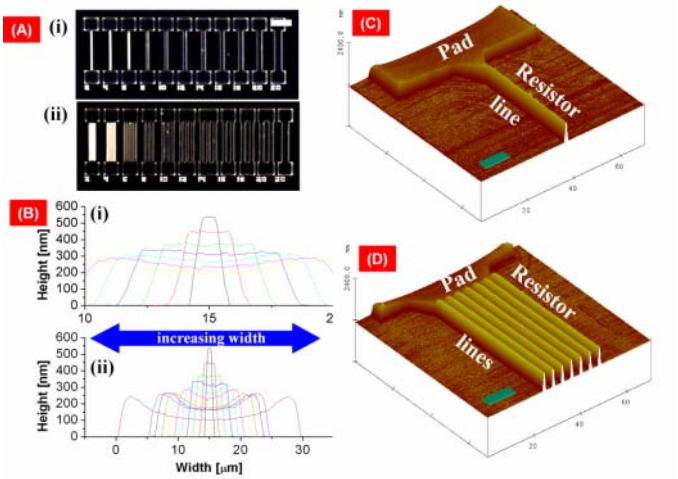


Figure 9. Nanoimprinted gold resistors. (A) Optical dark field images of (i) single and (ii) multi line resistors. Inset scale bar corresponds to 100 μm. (B) AFM cross section images of single gold resistors with diverse widths and (i) magnified view. AFM topography image of (C) a single line resistor and (D) a multiple line resistor. Inset scale bar corresponds to 10 μm.

The organic field effect transistors (OFETs) fabricated in this work have a typical bottom gate/bottom contact coplanar transistor configuration (Figure 10(B)) wherein the channel length is defined by the separation between the two parallel electrodes (source and drain) on top of the $SiO_2$/P+ Si wafer gate. Carboxylate-functionalized polythiophene (Figure 10(B) top inset) with increased air stability [17] was synthesized, dissolved in warm (>45 °C) 1,2-dichlorobenzene (*o*-DCB) solvent (3 mg/mL) and spincoated as an active layer.

Two types of transistor test configurations - single channel transistors shown in Figure 10(A) - i (optical dark field image) and Figure 10(C) (AFM topography) and multiple channel transistors shown in Figure 10(A)-ii(optical dark field image) and Figure 10(D) (AFM topography) – were fabricated by direct nanoimprinting. Figure 10(A) shows single channel transistors with various channel lengths (Figure10 (B)-i, 2/4/6/8/10/12/16/20/30/50 μm from left) and 160 μm channel width and multiple channel transistors with longer effective channel width (Figure10 (B)-ii, 800 μm for 2~6 μm channel and 480 μm for 8~50 μm channel) with same channel length.

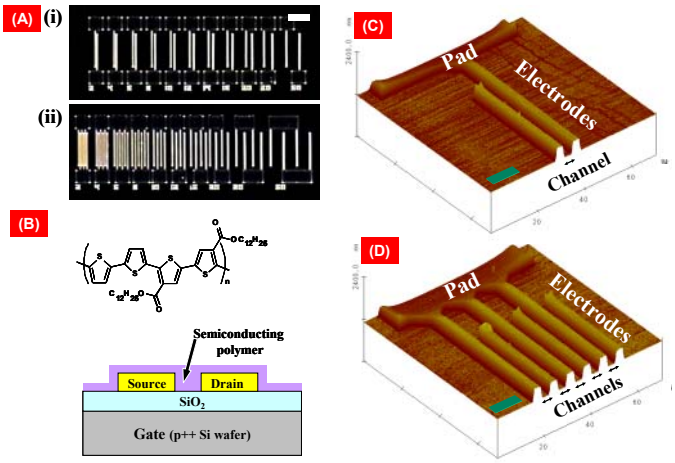


Figure 10. Nanoimprinted OFET with airstable semiconducting polymer. (A) Optical dark field images of (i) single and (ii) multi channel transistors. Inset scale bar corresponds to 100μm. (B) Schematics of OFET. Top inset is the the graphic formula of air stable carboxylate-functionalized polythiophene semiconducting polymer. AFM topography image of (C) a single channel OFET and (D) a multiple channel OFET with big contact pads. Inset scale bar corresponds to 10μm.

The OFETs performance was characterized using HP4155A semiconductor parameter analyzer and a probe station with the micro-positioning manipulators in a dark Faraday cage in air. The transfer and output characteristics of the OFETs are shown in Figure 11 for different channel lengths. The OFET with relatively longer channel (Figure 11(A) , $L$~4 μm, $W$~160 μm) shows typical output and transfer characteristics with operation in p-type accumulation mode with $I_{on}/I_{off}$ ratio of $10^3$~$10^4$ and threshold voltage ($V_t$) of -25 V while the OFET with relatively shorter channel (Figure 11(B) , $L$~800 nm, $W$~160 μm) exhibited output characteristics with similar $I_{on}/I_{off}$ ratio, but without current saturation, lower threshold voltage ($V_t$) of -15 V and much larger drain current. This so-called short channel effect is caused by several reasons [18]. The mobility extracted from the saturated transfer characteristics [17] of the OFET was found to be around 0.004~0.006 $cm^2/V \cdot s$. The nanoparticle nanoimprinting can produce very short channels (micron to submicron) with high drain current. The resolution of the fabricated OFET is determined by the original mold. Even submicron channels could be defined with a nanomold fabricated by e-beam lithography to achieve reduction of the channel length to improve switching speed.

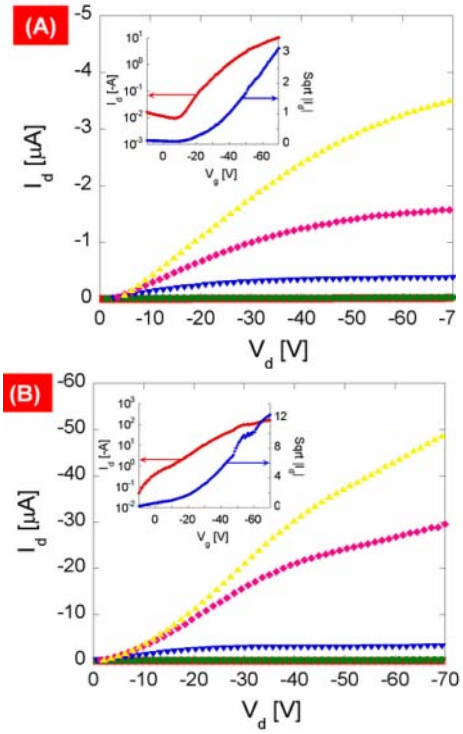


Figure 11. Output and transfer characteristics of OFET with long channel ((A), L~ 4μm) and short channel ((B), L~ 800 nm) with 160μm channel width. For output characteristics measurement, the drain voltage ($V_d$) was scanned from 0 to –70 V and the drain current ($I_d$) was measured while gate voltage ($V_g$) was fixed at -70,-50,-30,-10,10 V during each $V_d$ scanning. For transfer characteristics measurement (insets), $V_g$ was scanned from 10 to –70 V and the drain current ($I_d$) was measured while $V_d$ was fixed at –70 V.

## CONCLUSION

We developed a novel direct nanoimprinting process of metallic and semiconductor nanoparticles with low temperature and pressure requirement. Our approach provides a superior patterning performance in micro and nanoscale and can be used as an inexpensive and high-throughput nanopatterning method alternative to other expensive and low-throughput tools. We demonstrated nanoimprinting of gold (Au), silver (Ag), and cadmium selenide-zinc sulfide (CdSe-ZnS core-shell) quantum dots with features from microns down to 150nm resolution. Also, functional electronic devices such as organic field effect transistor (OFET) devices fabricated by direct nanoimprinting of metal nanoparticles have shown a successful device performance.

## ACKNOWLEDGMENTS

The authors wish to thank to Professor J.M.J Fréchet and Dr. C. Luscombe of Department of Chemistry, University of California, Berkeley for valuable discussions and material. We also give our thanks to Dr. Eung-Sug Lee and Dr. Jun-Ho Jeong at Korea Institute of Machinery and Materials (KIMM), Korea for helpful technical advices. Financial supports to the University of California, Berkeley by the U.S. National Science Foundation (Grant No. CTS-0417563) and Center for Nanoscale Mechatronics and Manufacturing (Grant No. 019997), one of the 21st Century Frontier Research Programs from Ministry of Science and Technology, Republic of Korea are gratefully acknowledged.

## REFERENCES

[1] Trucskett, V.N.; Watt, M.P.C. *Trends in biotechnology* **2006**, *24(7)*, 312-317.

[2] Nakamatsu K.; Matsui, S. *Japanese J. Appl. Phys.*, **2006**, *45(21)*, L546-548.

[3] Seekamp, J.; Zankovych, S.; Helfer, A. H.; Maury, P.; Sotomayor Torres, C.M.; Boettger, G.; Liguda, C.; Eich, M.; Heidari, B.; Montelius, L.; Ahopelto, J. *Nanotechnology* **2002**, *13(5)*, 581-586.

[4] Wu, W.; Jung, G-Y.; Olynick, D.; Straznicky, J.; Li, Z.; Li, X.; Ohlberg, D.; Chen, Y.; Wang, S-Y.; Liddle, J.; Tong, W.; Williams, R.S., *Appl. Phys. A* **2005**, *80(6)*, 1173-1178.

[5] Kim, C.; Stein, M.; Forrest, S.R. *Appl. Phys. Lett.* **2002**, *80*, 4051-4053.

[6] Clavijo-Cedeño, C.; Seekamp, J.A.; Kam, P.; Hoffmann, T.; Zankovych, S.; Sotomayor Torres, C.M.; Menozzi, C.; Cavallini, M.; Murgia, M.; Ruani, G.; Biscarini, F.; Behl, M.; Zentel, R.; Ahopelto, J. *Microelectronic Eng.* **2002**, 61-62, 25-31.

[7] Park, I.; Cheng, J.; Pisano, A.P.; Lee, E.; Jeong, J. *Appl. Phys. Lett.* **2007**, *90*, 093902(1-3).

[8] Schultz, D.A., Curr. Opin. Biotechnol. **2003**, 14, 13-22.

[9] Sotomayor Torres, C.M. *Alternative Lithography*; Springer, New York, 2003.

[10] Yoshihiko, H.; Toshihiko, U.; Tomohiro, K.; Takashi, M. *Proc.SPIE* **2003**, *5220*, 74-81.

[11] Chen, H.L.; Chuang, S.Y.; Cheng, H.C.; Lin, C.H.; Chu, T.C. *Microelectronic Eng.* **2006**, *83*, 893-896.

[12] Ko, S.H.; Park, I.; Pan, H.; Grigoropoulos, C.P.; Pisano, A.P.; Luscombe, C.K.; Frechet, J.M.J., *Nano Lett.* **2007**, *7,*1869-1877.

[13] Kim, E.; Xia, Y.; Zhao, X.; Whitesides G.M. *Adv. Mater.* **1997**, 9, 651-654.

[14] Medintz, I.L.; Uyeda, H.T.; Goldma, E.R.; Mattoussi, H., *Nat. Mater.* **2005**, *4*, 435-446.

[15] Hostetler, M.J.; Wingate, J.E.; Zhong, C.J.; Harris, H.E.; Vachet, R.W.; Clark, M.R.; Nondono, J.D.; Green, S.J.; Stokes, J.J.; Wignall, G.D.; Glish, G.L.; Porter, M.D.; Evans, N.D.; Murray, R.W. *Langmuir* **1998**, *14(1)*, 17-30.

[16] Chung, J.; Bieri, N.R.; Ko, S.; Grigoropoulos, C.P.; Poulikakos, D. *Appl. Phys. A.* **2004**, *79*, 1259-1261.

[17] Scheer, H.C.; Schulz, H. *Microelectronic Eng.* **2001**, *56*, 311-332.

[18] Pierret, R.F. *Semiconductor Device Fundamentals*, Addison Wesley, New York, **1996.**